Journal of
Micropalaeontology
Open Access

Population morphometrics of the Southern Ocean diatom *Fragilariopsis kerguelensis* related to sea surface temperature

Joseph A. Ruggiero[1,a], **Reed P. Scherer**[1], **Joseph Mastro**[1], **Cesar G. Lopez**[1,2], **Marcus Angus**[1,3], **Evie Unger-Harquail**[4], **Olivia Quartz**[4], **Amy Leventer**[4], **and Claus-Dieter Hillenbrand**[5]

[1]Department of Earth, Atmosphere and Environment, Northern Illinois University, DeKalb, IL 60115, USA
[2]Department of Earth, Environmental, and Planetary Sciences,
Washington University, St. Louis, MO 63130, USA
[3]Department of Geology, University of Nevada, Reno, Reno, NV 89557, USA
[4]Department of Earth and Environmental Geosciences, Colgate University, Hamilton, NY 13346, USA
[5]British Antarctic Survey, Cambridge, UK
[a]present address: Department of Geology and Geological Engineering,
Colorado School of Mines, Golden, CO 80401, USA

Correspondence: Joseph A. Ruggiero (joseph.a.ruggiero@gmail.com)

Abstract. With the onset of anthropogenic climate change, it is vital that we understand climate sensitivity and rates of change during periods of warming in the Earth's past to properly inform climate forecasts. To best inform modeling of ongoing and future changes, environmental conditions during past periods of extreme warmth are ideally developed from multiproxy approaches, including the development of novel proxies where traditional approaches fail. This study builds on a proposed sea surface temperature (SST) proxy for the high-latitude Southern Ocean, based on the morphometrics of the ubiquitous Antarctic diatom *Fragilariopsis kerguelensis*. This species has been shown to display two distinct morphotypes; a low-rectangularity morphotype is interpreted to be more common in warmer waters while a high-rectangularity morphotype is more common in cooler waters. The proportion of the low-rectangularity morphotype (pLR) has been correlated to SST and summer SST (SSST). Here, we examine this proxy by reconstructing SST using sediment samples from the modern seafloor surface in the Amundsen Sea and the Sabrina Coast to test how well two published calibrations of this relationship (Kloster et al., 2018; Glemser et al., 2019) reconstruct SST and SSST in the modern ocean. In the Amundsen Sea surface sediments, we calculate derived SST -1.6 to $-1.2\,°C$ and derived SSST 0.6 to 0.7 °C. In the Sabrina Coast surface sediments, we calculate derived SST -0.3 to 0.5 °C and derived SSST 1.4 to 2.5 °C. We discuss the differing population dynamics of *F. kerguelensis* in our surface samples between the Amundsen Sea and Sabrina Coast because the Amundsen Sea specimens display a lower pLR than Sabrina Coast specimens, although they exist in warmer waters and should display a higher pLR. We also use the two published calibrations to preliminarily reconstruct SST and SSST in the Amundsen Sea over the last interglacial, Marine Isotope Stage 5 (MIS-5). We calculate SSTs that are slightly cooler or within the range of the modern Amundsen Sea for the duration of the last interglacial; we calculate summer SSTs $\sim 1\,°C$ warmer than the modern Amundsen Sea. This suggests MIS-5 SSTs were at most marginally warmer than the modern Amundsen Sea.

1   Introduction

Modern ocean warming and the enhanced upwelling of Circumpolar Deep Water (CDW) near the West Antarctic continental margin has been shown to be a significant threat to ice sheet stability to an even greater extent than atmospheric warming (Holland et al., 2020). This ocean forcing has the potential to destabilize the ice streams draining the West Antarctic Ice Sheet (WAIS), which is grounded to as much as 2500 m below sea level (e.g., Seroussi et al., 2017; Morlighem et al., 2020; Patterson et al., 2022). To better inform forecasts of future ice sheet changes, it is necessary to understand the environmental conditions during previous warming periods of Earth's history. We study past sea surface temperature (SST) in the Southern Ocean using marine proxies. Model simulations have shown that, like at present, seawater temperatures are particularly important in driving grounding line retreat and ice sheet thinning (e.g., DeConto and Pollard, 2016), which has been corroborated by proxy data from marine sediment records (e.g., Hillenbrand et al., 2017). Although it is mainly the ocean heat supplied by CDW that forces WAIS retreat (DeConto and Pollard, 2016; Holland et al., 2020), paired stable carbon isotope ($\delta^{13}C$) data from planktic and benthic foraminifera in Holocene sediments from the Amundsen Sea shelf have revealed that changes in CDW temperature and/or upwelling also leave a corresponding signal in the surface water (Hillenbrand et al., 2017). This is consistent with modern observations from the Antarctic Pacific margin showing that increased CDW advection also increases the near surface ocean heat content (Martinson et al., 2008). Past SST, along with other environmental conditions, is best reconstructed using multi-proxy approaches that allow for cross-verification to fill gaps that may be due to seasonal influence of different proxies. Although several SST proxies have been applied to Neogene to Quaternary Southern Ocean sediments, there is need for novel proxy development because material for study remains scarce, and no existing proxy is universally applicable to all available sediment types (Kim et al., 2009; Ho et al., 2014; Mollenhauer et al., 2015; Fietz et al., 2016; de Bar et al., 2020; Inglis and Tierney, 2020).

Fragilariopsis kerguelensis is a heavily silicified diatom species that dominates marine sediments in the southern high latitudes. *F. kerguelensis* evolved in the early Pleistocene and became the dominant diatom of the Southern Ocean during the mid-Pleistocene (Cortese and Gersonde, 2008; Cortese et al., 2012; Kloster et al., 2017). Computer-aided morphologic studies of *F. kerguelensis* demonstrate that its morphology ranges from being narrowly elliptic to lanceolate, which is defined as having high or low rectangularity, respectively (Kloster et al., 2018). This morphologic distinction has been shown to correlate with several environmental variables, including iron input, sea ice duration, length of growing season, location of the Antarctic Polar Front, and light levels, but the strongest and most consistent correlation in earlier studies

is to the SST under which the populations grew (Cortese and Gersonde, 2007; Crosta, 2009; Cortese et al., 2012; Shukla et al., 2013; Shukla and Crosta, 2017; Glemser et al., 2019). With further confirmation of this correlation, *F. kerguelensis* morphology may provide a meaningful SST proxy in the high-latitude Southern Ocean.

F. kerguelensis populations in the Weddell and Bellingshausen seas have previously been shown to display a mixture of two morphologic populations based on the measured valve rectangularity (R); proportions of the two modalities (low rectangularity and high rectangularity) have been correlated with SST (Kloster et al., 2018; Glemser et al., 2019). *F. kerguelensis* populations that display a relatively high proportion of a low-rectangularity valves (pLR) have been documented living in relatively warm surface waters (1–5 °C) and preserved in underlying seafloor surface sediments, whereas populations that display a lower pLR have been documented living in colder surface waters ($< \sim 1$ °C) and preserved on the underlying seabed (Kloster et al., 2018; Glemser et al., 2019). These findings provide an impetus for paleo-SST reconstruction using this SST–valve morphology relationship (Fig. 1).

Two recent studies have explored this relationship, resulting in two different SST and valve morphology proxy estimates. The study of Kloster et al. (2018) is an initial exploration into using relative rectangularity abundances to reconstruct paleo-temperatures. In their study, a low valve rectangularity to high valve rectangularity ratio was calculated and compared to Antarctic summer sea surface temperature (SSST) reconstructed through the past ca. 140 000 years via transfer functions by Esper and Gersonde (2014), finding that the presence of the low-rectangularity class correlated well with SSST. By comparing the rectangularity of *F. kerguelensis* populations in downcore intervals from the Weddell Sea to SST calculations derived from diatom transfer functions performed on the same core intervals, the study inferred Eq. (1) for reconstructing SSST (in °C) (Kloster et al., 2018), in which LR/HR represents the ratio of low-rectangularity to high-rectangularity valves in a sample population (unitless):

$$\text{SSST} = 0.215 \cdot \left[\frac{\text{LR}}{\text{HR}} \right] + 0.512. \tag{1}$$

Glemser et al.'s (2019) study expands on this *F. kerguelensis* valve morphology control, along with other environmental controls, and examines if both low- and high-rectangularity morphotypes appear in recent water column and surface sediment assemblages using the proportion of low-rectangularity (pLR) valves relative to valves of the entire population as a measure of annual SST change. In their study, they collected *F. kerguelensis* samples with net hand catches along three separate transects, PS40, PS79 and PS103, in the Atlantic sector of the Southern Ocean and plotted frustule rectangularity against modern ocean temperatures from World Ocean Atlas (2009). In addition, the authors analyzed *F. kerguelensis* frustules of seafloor surface sediment samples along one
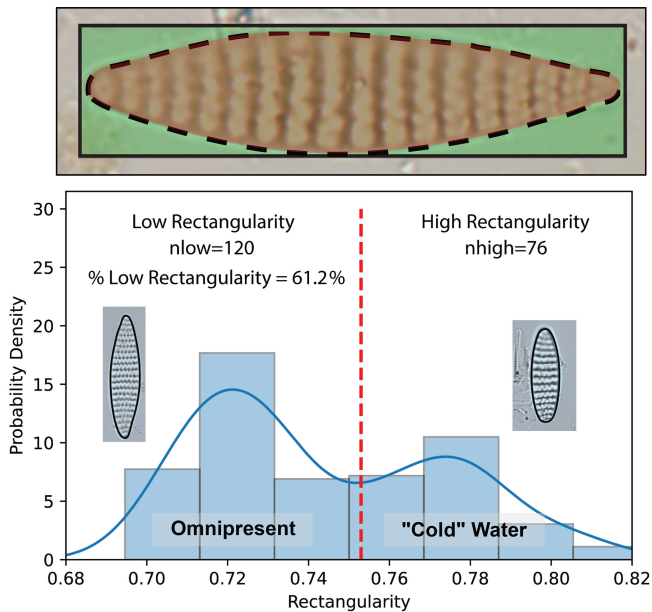
Figure 1. The top panel shows an illustration of *Fragilariopsis kerguelensis* rectangularity. The red-shaded oval shows the area of the valve inside of the green-shaded rectangle. The bottom panel shows an example distribution of an *F. kerguelensis* assemblage in sediment showing low rectangularity (left) and high rectangularity (right).

transect, PS35, in the Pacific sector of the Southern Ocean, where rectangularity correlated less well with modern SSTs. They found that there is a strong initial gradient in pLR below 0 °C, but above 0 °C pLR leveled out. SST is described by Eq. (2) (Glemser et al., 2019):

$$\log\left(\frac{\text{pLR}}{1\text{-pLR}}\right) = 0.125 + 2.10 \cdot \log(\text{SST} + 2). \tag{2}$$

The study presented in this article uses these functions to quantify SST and SSST in surface sediments from the Amundsen Sea and Sabrina Coast to examine whether they reflect true temperatures in these locations. We also characterize and compare *F. kerguelensis* assemblages between the Amundsen Sea and Sabrina Coast. Finally, we quantify SST and SSST in Amundsen Sea sediments from the last interglacial, Marine Isotope Stage 5 (MIS-5) using the two described equations.

2 Materials and sample preparation methods

Fragilariopsis kerguelensis specimens analyzed in this study were collected from the Amundsen Sea and Sabrina Coast in seafloor surface and downcore sediments (Fig. 2, Table 1). The modern Amundsen Sea samples include core top sediment samples from piston core PC496 and box core BC495 recovered on RRS *James Clark Ross* expedition 179 (JR179) in 2008 (Enderlein and Larter, 2008). In addition, we ana-

lyzed *F. kerguelensis* valves settled from core bottom water on the top of core U1532A-1H recovered on International Ocean Discovery Program Expedition 379 (IODP Exp379) in 2019 (Gohl et al., 2021). This sample is made up of suspended sediment in the core barrel of the first penetration and represents the late Holocene; it is probably comprised of a mixture of diatoms representing the last several thousand years. While the upper sediments in a piston core may have some preservation issues and the core water would ideally not be used as a representation for "modern" deposition, devout surface sediment samples such as box core or multicore were not collected in these sites, so we use core top from PC496 and core bottom water from U1532A as stand ins for "modern" sedimentation. The collection of these samples may provide a yet unquantified bias to analytical results. The down-core sediment samples from the Amundsen Sea include 19 samples from 114–262 cm depth in core PC496; 18 samples were analyzed from 140–370 cm depth in core U1533D-1H, which was also recovered during IODP Exp379 (Gohl et al., 2020). According to age models developed by Horrocks (2018) and Hopkins et al. (2024), these sediments span the last interglacial period, i.e., Marine Isotope Stage (MIS) 5 from 130 to 71 ka (Lisiecki and Raymo, 2005). Both core PC496 and the two IODP Exp379 cores were recovered from sediment drifts on the Amundsen Sea continental rise (Uenzelmann-Neben and Gohl, 2012; Horrocks, 2018; Gohl et al., 2021). Seafloor surface sediments from the Sabrina Coast were collected on expedition IN2017-V01 (samples from multi-cores MC01, MC02, MC03, MC04, MC05) with RV *Investigator* in 2017 and on expedition NBP1402 with RV/IB *Nathaniel B Palmer* expedition in 2014 (samples from mega-cores MC45, and MC61). The core tops and box cores from both the Amundsen Sea and Sabrina Coast ideally represent modern deposition, and we assume *F. kerguelensis* assemblages preserved in these sediments to represent the modern ocean.

F. kerguelensis specimens were manually identified and imaged using a Leica DMLV optical microscope from strewn or settled slides mounted in Norland-61 optical adhesive, following Warnock and Scherer (2015). Effort was taken to make the perimeter of each valve as bold as possible for image processing to identify. Each image was then inputted into SHERPA (Shape Recognition, Processing and Analysis) image processing software (Kloster et al., 2014). SHERPA is compatible with slide-scanning microscopes, meaning that an automatic or semi-automatic workflow is often possible. However, we found that it is also possible to perform shape analysis using this software in a completely manual fashion in which images are manually inputted, edited and measured. SHERPA analyses and measures the shape in question for a number of descriptors including rectangularity, but it does not always accurately capture the desired valve, often capturing sediments that overlapped the valve as part of the diatom valve itself. Thus, each image had to be manually edited to properly fit this shape of the imaged valve. This en-

Table 1. Sample site locations and usage.

Expedition	Sample name*	Region	Longitude	Latitude	Type	Usage**	Depth (cm)
JR179	BC495	Amundsen Sea	−108.34936	−70.04879	Box Core	SSA	0–1
JR179	PC496	Amundsen Sea	−106.68016	−69.23008	Piston Core	SSA, MIS-5	0–4/downcore
IODP379	U1532	Amundsen Sea	−107.5255	−68.61139	Core Top Bottom Water	SSA	Core Water
IODP379	U1533	Amundsen Sea	−109.03223	−68.73571	IODP adv. Piston core	MIS-5	downcore
IN2017	MC01	Sabrina Coast	115.623	−64.471	Multi-core	SSA	0–1
IN2017	MC02	Sabrina Coast	115.043	−64.463	Multi-core	SSA	0–1
IN2017	MC03	Sabrina Coast	119.301	−64.675	Multi-core	SSA	0–1
IN2017	MC04	Sabrina Coast	119.018	−64.654	Multi-core	SSA	0–1
IN2017	MC05	Sabrina Coast	118.696	−64.729	Multi-core	SSA	0–1
NBP1402	MC45	Sabrina Coast	120.5	−66.183	Multi-core	SSA	0–1
NBP1402	MC61	Sabrina Coast	120.464	−66.128	Multi-core	SSA	0–1

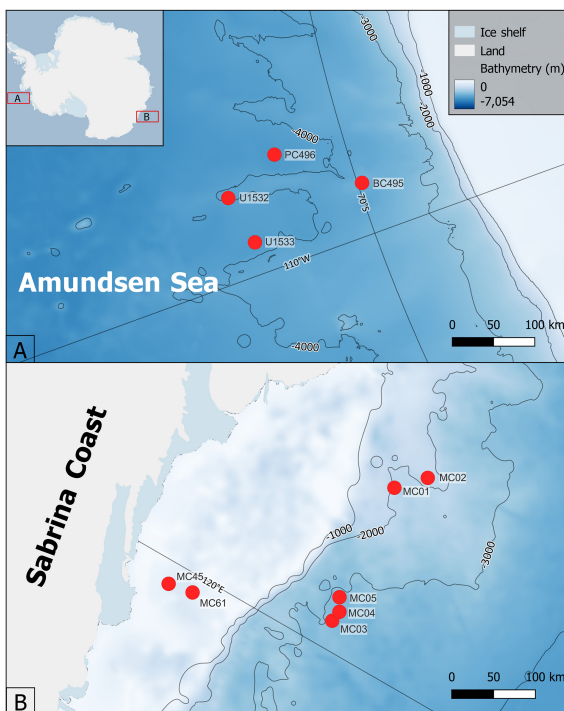* Name as referred to in paper. ** SSA stands for surface sediment analysis.

Figure 2. Site map of sample locations used in this study: **(a)** Amundsen Sea core locations and **(b)** Sabrina Coast core locations. Surface sediments were used in all study locations except for U1533. This study also examined downcore sediments that cover the MIS-5 interval of cores U1532 and U1533 in the Amundsen Sea. Map generated using Quantarctica3 (Matsuoka et al., 2021).

sured that each image taken was of an *F. kerguelensis* valve and that SHERPA properly measured the area each valve. At least *n* = 150 *F. kerguelensis* specimens were analyzed per sample, and rectangularity values were calculated based on Eq. (3) after Droop (1995).

$$\text{Rectangularity} = \frac{\text{area of valve}}{\text{area of enclosing rectangle}} \quad (3)$$

Rectangularity data for each of the specimens was imported into a .csv file, where each specimen was designated either "low rectangularity" or "high rectangularity". High- or low-rectangularity valves are distinguished by a threshold rectangularity of 0.751. It is possible that this distinguishing number will be different for different populations of *F. kerguelensis* around the Southern Ocean (Kloster et al., 2018; Glemser et al., 2019), but we decided to maintain this threshold to align with the previous two studies. The proportion of low-rectangularity valves (pLR) in each population was calculated and entered into the defined equations that reflect the SST–valve morphology relationship, allowing us to calculate SST for that specific *F. kerguelensis* population. Simple length/width ratios can be highly variable, depending on the size of the initial post auxosporulation cell and the stage number of subsequent cell divisions, meaning a sample population might display a variety of valve sizes regardless of environmental conditions. By contrast, rectangularity measurements have been shown to be consistent, regardless of overall valve area, as it is unitless and accounts for generational diminishing of valve area, typically preserving the overall shape of the frustule (Kloster et al., 2018).

3 Results

3.1 Derived SST and SSST from Amundsen Sea and Sabrina Coast surface sediments

We use the two existing calibrations (Kloster et al., 2018; Glemser et al., 2019) to reconstruct SST and SSST in core tops for Amundsen Sea sites PC496, BC495 and U1532 and surface sediment samples from the Sabrina Coast in samples MC01, MC01, MC03, MC04, MC05, MC45 and MC61 (Table 2, Figs. 3, 4) to represent a "modern" SST reconstruction. We then compare the Amundsen Sea results to modern SSST inferred from nearby in situ measurements given by the Quantarctica3 database, generated from the World Ocean Atlas (WOA) 2013, which provide a modern SSST range for

the sites of −0.5 (BC495) to 0.3 °C (U1532) on the continental slope where these samples were taken from (Locarnini et al., 2013). We also compare the Sabrina Coast results to CTD (conductivity, temperature, and depth) measurements taken by Bensi et al. (2022) and Orsi and Webb (2022), which provide SSSTs of −2 to −1 °C, and to Locarnini et al. (2013) SSST, which provides temperatures for the sites in question ranging from −1.2 (MC45) to 0.4 °C (MC03). Mean sea surface temperature (i.e., SST) is likely to be biased towards summer temperatures in the Southern Ocean as most of the empirical measurements used in the WOA are measured in the austral summer. Therefore, here we compare derived SST and SSST to WOA (2013) summer SST and winter SST to examine surface and downcore derived temperature in a non-biased way, although we do not compare directly them to "mean SST".

3.2 Biogeographic discrepancies between Amundsen Sea and Sabrina Coast *F. kerguelensis* Populations

We also characterized *F. kerguelensis* assemblages in Sabrina Coast and Amundsen Sea surface sediments. Here we present a comparison of these populations using the variability of statistical measures: mean, median, mode, skew and kurtosis (Table 3). We additionally speculate on the drivers for differences in *F. kerguelensis* population rectangularity in the Amundsen Sea and the Sabrina Coast.

F. kerguelensis valves in U1532 surface samples present distributions of moderate rectangularity values with means of 0.76 (pLR: 0.435; skew: 0.08; kurtosis: −0.248) and PC496 surface samples present distributions of moderate rectangularity with 0.758 (pLR: 0.448; skew: 0.113; kurtosis: −0.791). The BC495 population is weighted towards lower pLR with a mean of 0.776 (pLR: 0.141; skew: −0.686; kurtosis: 0.555). Sabrina Coast *F. kerguelensis* populations are generally weighted towards higher pLR. Means of Sabrina Coast *F. kerguelensis* populations range between 0.731 and 0.743, while skewness values range from −1.037 to 1.752 and kurtosis values range from 0.448 to 20.179.

3.3 Derived SST and SSST from Amundsen Sea MIS-5

We finally use the two calibrations to reconstruct SST through the MIS-5 interval in Amundsen Sea cores PC496 and U1533D-1H (hereafter U1533) (Fig. 5, Table 4). In PC496, we calculate derived-SSST across MIS-5 ranging from 0.6 to 1.1 °C and derived-SSTs ranging from −1.5 to −0.6 °C. Derived temperature fluctuates most in the middle of PC496 between 164 to 214 cm b.s.f. In U1533, we calculate derived SSST across MIS-5 ranging from 0.8 to 1.7 °C and derived SSTs ranging from −0.9 to −0.1 °C. The highest derived temperatures occur near the bottom of U1533 between 271 and 376 cm b.s.f.

4 Discussion

4.1 Reconstructing modern SST and SSSTs from *F. kerguelensis* in surface sediments

Modern Amundsen Sea SSTs generally range between −0.5 to 0.0 °C (World Ocean Atlas (WOA); Locarnini et al., 2013). Upon analysis of surface sediments in PC496 and BC495 and core water from U1532 (Table 2), we derive SSSTs that are warmer than this range (0.5 to 0.6 °C), but we derive SSTs that are colder than this range (−1.6 to −1.2 °C). It is logical that derived summer SSTs would be warmer than the annual average SST presented by the WOA. However, it is interesting that we derive colder SSTs than are present. We propose three possible explanations for colder than reported derived SST: (1) the temperature model is not sufficiently attuned to actual SST, (2) the microfossil record is biasing towards the cooler low-rectangularity morphotype or (3) the sediments sample we have designated "surface samples" are not actually modern as we operate under the assumption that surface sediments are a stand in for modern deposition. Point 3 could be rectified by radiocarbon dating surface sediments but points 1 and 2 will require a more in-depth study of *F. kerguelensis* population dynamics.

The surface waters off the Sabrina Coast generally range between −2 and −1 °C annually. We derive SSSTs between 1.4 to 2.5 °C in Sabrina Coast surface sediments, warmer than the yearly average. We also derive SSTs that range between −0.3 and −1.2 °C, still warmer than the presented yearly average. Interestingly, while our derived SST (via Glemser et al., 2019) in the Amundsen Sea is colder than the Amundsen Sea yearly average as reported by Locarnini et al. (2013), our derived SST in the Sabrina Coast is warmer than Locarnini et al. (2013) reported Sabrina Coast. Additionally, actual Sabrina Coast SSTs are ∼ 0.5 to 1.5 °C colder than Amundsen Sea SSTs. Based on our understanding of the SST–valve morphology relationship, this should mean that *F. kerguelensis* assemblages on the Sabrina Coast, as compared to the Amundsen Sea, would have proportionately fewer low-rectangularity valves with population rectangularity skewed more in favor of higher-rectangularity valves that are more prevalent in colder waters. However, the Sabrina Coast *F. kerguelensis* assemblages have proportionately more low-rectangularity valves and fewer high-rectangularity valves, which is why we derive warmer SSTs and SSSTs than those that exist. Clearly, there is some discrepancy between Amundsen Sea and Sabrina Coast *F. kerguelensis* populations that causes a high pLR in the relatively colder waters of the Sabrina Coast when there should be a lower pLR. We propose that this discrepancy is due to a fundamental difference between Amundsen Sea and Sabrina Coast *F. kerguelensis* populations, which we discuss in Sect. 4.2.

Table 2. Derived SST and SSST from surface sediments in the Southern Ocean.

Amundsen Sea								
Cruise	Core	Depth	SSST (WOA, 2013)	WSST (WOA, 2013)	No. of LR/ no. of HR ratio	SSST °C via Kloster et al. (2018)	pLR	SST °C via Glemser et al. (2019)
JR179	BC495	0–1	−0.5	−1.4	0.811	0.7	0.141	−1.2
JR179	PC496	0–4	−0.1	−1.2	0.165	0.6	0.448	−1.6
IODP379	U1532	Core Water	0.3	−1.1	0.435	0.7	0.435	−1.2
Sabrina Coast								
IN2017	MC01	0–1	−0.1	−1.7	7.100	2.0	0.877	0.2
IN2017	MC02	0–1	−0.2	−1.7	5.077	1.6	0.835	−0.1
IN2017	MC03	0–1	−0.4	−1.0	6.524	1.9	0.867	0.1
IN2017	MC04	0–1	0.4	−1.0	9.400	2.5	0.904	0.5
IN2017	MC05	0–1	0.0	−1.0	4.241	1.4	0.809	−0.3
NBP1402	MC45	0–1	−1.2	−1.4	3.903	1.4	0.796	−0.3
NBP1402	MC61	0–1	−1.1	−1.4	4.440	1.5	0.816	−0.2

No. of LR/no. of HR ratio is the number of low-rectangularity valves divided by the number of high-rectangularity valves, pLR is the proportion of low rectangularity, SSST is the summer sea surface temperature, and WSST is the winter sea surface temperature.
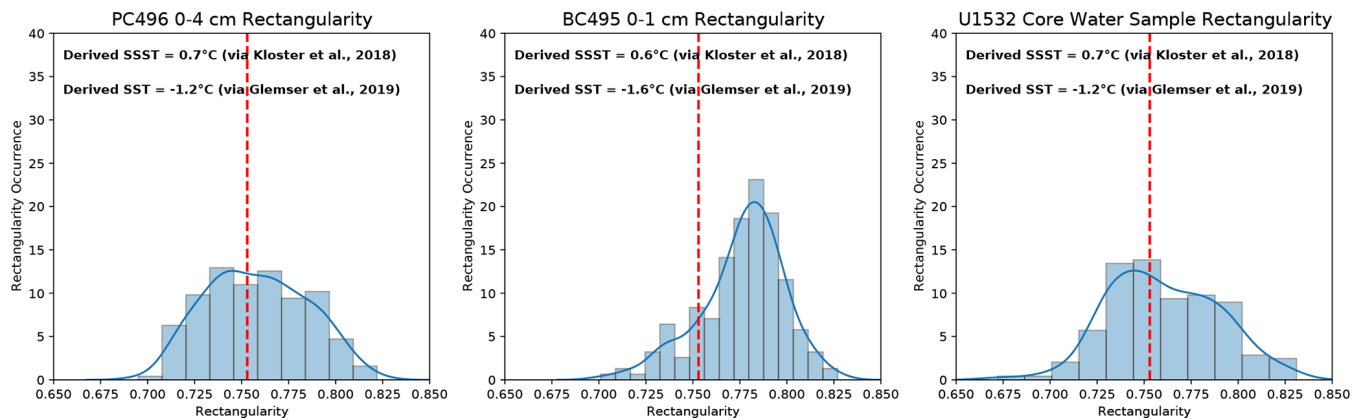

Figure 3. Derived SST and SSST and population rectangularity distributions from *F. kerguelensis* specimens in Amundsen Sea surface sediment samples. Modern SSST ranges between −0.5 to 0.3 °C for these sites.

4.2 *F. kerguelensis* population dynamics in the Amundsen Sea vs. Sabrina Coast

Here we discuss similarities and differences between *F. kerguelensis* populations preserved in Amundsen Sea and Sabrina Coast sediments. In the surface sediments from the Amundsen Sea, we find *F. kerguelensis* populations that display both high and low rectangularity types, although these populations often trend unimodal and range across the 0.751 threshold. Kloster et al. (2018) found several *F. kerguelensis* assemblages from glacial periods as having bimodal populations, in which an assemblage displays both rectangularity morphotypes as two distinct populations and found assemblages from interglacial periods as having unimodal populations, in which assemblages trend more towards a single morphotype. An analysis of *F. kerguelensis* in seawater and sediment samples from the Weddell and Bellingshausen

seas found the presence of the two morphotypes in both live catches and surface sediment assemblages (Glemser et al., 2019). Our investigations reveal that *F. kerguelensis* populations in surface sediments from both the Amundsen Sea and Sabrina Coast lack this bimodal morphology and display a largely unimodal morphology trending towards a single morphotype, albeit a unimodal morphology that displays both high- and low-rectangularity morphotypes according to the predetermined threshold.

In a normal distribution, the mean is equal to the median and the mode. Skewness represents the amount of asymmetry in a normal distribution. In this study, skew being equal to 0 means the distribution is symmetrical and the population is centered around the threshold of 0.751 (this theoretically separates high- and low-rectangularity populations; Kloster et al., 2018). Skew < 0 means data points are more concentrated on high-rectangularity specimens,
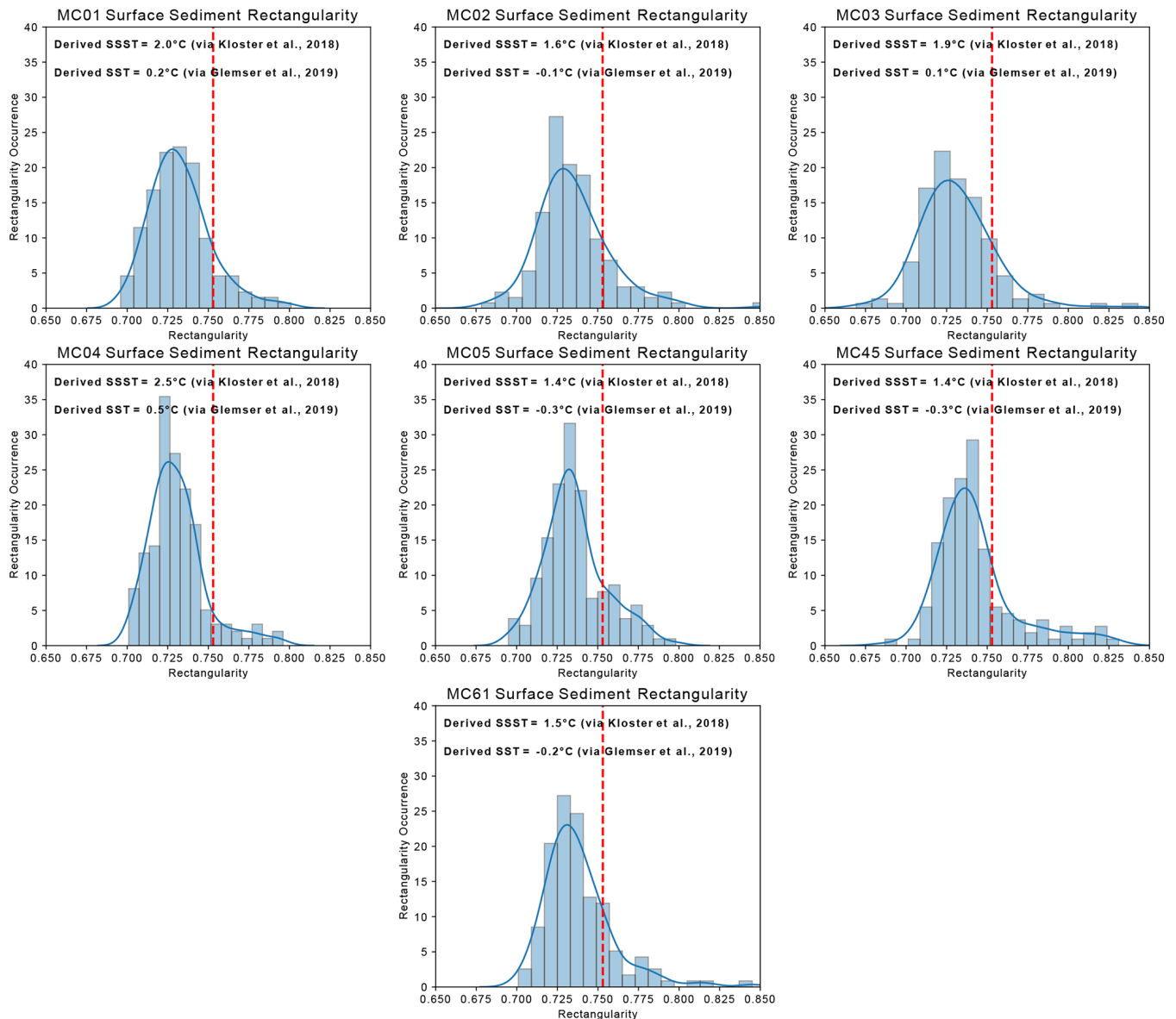
Sabrina Coast Surface Sediments

Figure 4. Derived SST and SSST and population rectangularity distributions from *F. kerguelensis* specimens in Sabrina Coast surface sediment samples. Modern SSST is ~ -2.0 to $-1\,°C$ (Bensi et al., 2022; Orsi and Webb, 2022) for the Sabrina Coast generally or -1.2 to $-0.4\,°C$ (Locarnini et al, 2013) for these sites.

and skew > 0 means data points are more concentrated on low-rectangularity specimens. Excess kurtosis describes the "tailedness" of data, which represents how often outliers in data occur; here, we use kurtosis to determine whether the tails of a distribution contain extreme values and how far data ranges from the mean. Normal distributions will have kurtosis of 0, distributions in which kurtosis > 0 (positive excess kurtosis) indicate large outliers in the data, distributions in which kurtosis < 0 (negative excess kurtosis) indicate small outliers in the data. Low kurtosis signifies most data will be

found close to the mean while high kurtosis signifies data will be found further from the mean. In this context, high kurtosis signifies that *F. kerguelensis* valve rectangularity values range more widely and further from the mean as compared to a population with low kurtosis in which rectangularity values cluster closely to the mean and most valves in a population are alike in rectangularity.

The observed assemblages either trend towards moderate rectangularity observed in the samples from cores PC496 (mean: 0.758; skew: 0.113; kurtosis: -0.791) and U1532

Table 3. *F. kerguelensis* population descriptors in surface sediments.

Amundsen Sea

Cruise	Core	Depth	Longitude	Latitude	No. of specimens	Mean	Median	Mode	SD	Skew	Kurtosis
JR179	BC495	0–1	−108.3494	−70.04879	198	0.776	0.780	0.784	0.022	−0.686	0.555
JR179	PC496	0–4	−106.6802	−69.23008	201	0.758	0.757	0.742	0.026	0.113	−0.791
IODP379	U1532	Core water	−107.5255	−68.61139	170	0.760	0.757	0.730	0.029	0.080	−0.284

Sabrina Coast

Cruise	Core	Depth	Longitude	Latitude	No. of specimens	Mean	Median	Mode	SD	Skew	Kurtosis
IN2017	MC01	0–1	115.623	−64.471	162	0.733	0.730	0.729	0.019	0.87	1.228
IN2017	MC02	0–1	115.043	−64.463	158	0.733	0.732	0.722	0.028	−1.037	10.297
IN2017	MC03	0–1	119.301	−64.675	158	0.731	0.729	0.722	0.032	−0.244	20.179
IN2017	MC04	0–1	119.018	−64.654	156	0.731	0.728	0.721	0.017	1.282	2.350
IN2017	MC05	0–1	118.696	−64.729	152	0.736	0.734	0.731	0.019	0.651	0.488
NBP1402	MC45	0–1	120.5	−66.183	152	0.743	0.738	0.742	0.025	1.456	2.345
NBP1402	MC61	0–1	120.464	−66.128	147	0.738	0.734	0.740	0.021	1.752	4.988
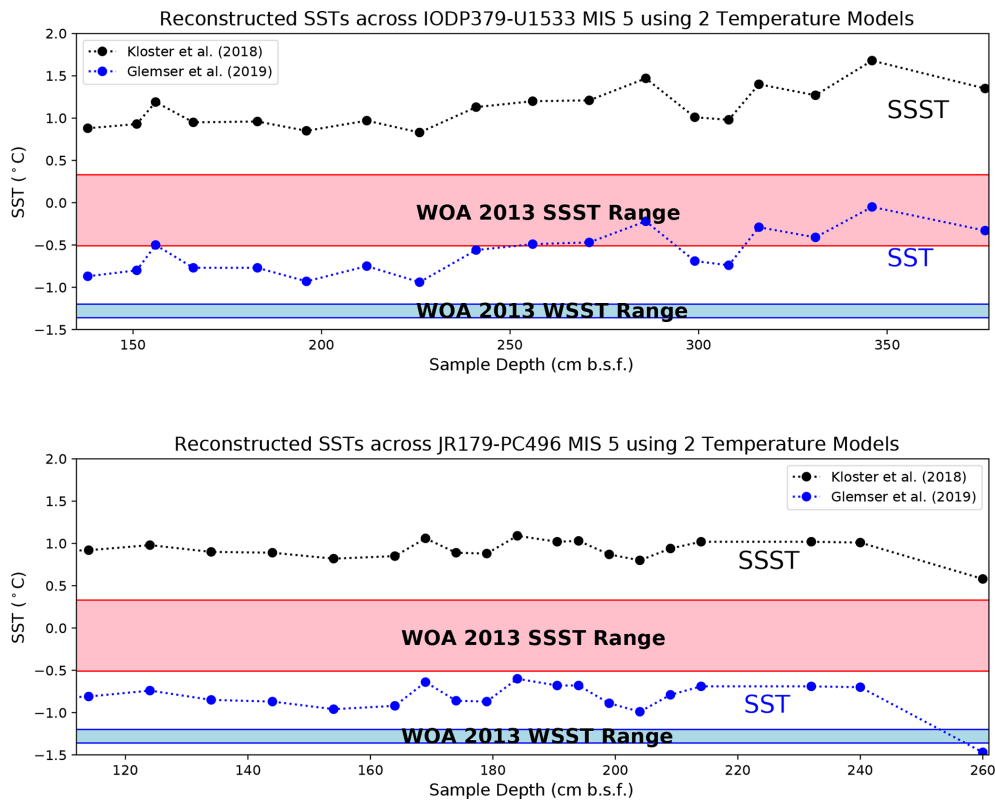
Figure 5. Reconstructed SST and SSST for cores PC496 and U1533 across MIS-5 using calibrations published by Kloster et al. (2018) and Glemser et al. (2019). We compare the results from the two models to the modern Amundsen Sea SSST (−0.5 to 0.3 °C) range and winter SST (WSST) range (−1.4 to −1.1 °C) from Locarnini et al. (2013).

core water (mean: 0.760; skew: 0.080; kurtosis: −0.248) or are skewed towards high-rectangularity valves as observed in the surface sediment at site BC495 (mean: 0.776; skew: −0.686; kurtosis: 0.555) (Table 3). The skew and kurtosis descriptors in PC496 and U1532 suggest that most individuals in the population are closely clustered around the moderate-rectangularity mean of 0.751. The negative skew found for *F. kerguelensis* specimens in BC495 suggests that

this population is skewed towards high rectangularity valves, but the low kurtosis value suggests the population is still mostly clustered around the higher rectangularity mean of 0.776. These statistics indicate that these three populations are close to normal populations (skew and kurtosis = 0; mean = median = mode). The pLR values in the Amundsen Sea populations range from 14.1–44.8 pLR. All three of these populations visually do not present the two separate high-

Table 4. Derived SST and SSST from the MIS-5 Amundsen Sea.

PC496			U1533		
Depth (cm)	SST*	SSST**	Depth (cm)	SST*	SSST**
114	−0.8	0.9	138	−0.9	0.5
124	−0.7	1.0	151	−0.8	0.5
134	−0.8	0.9	156	−0.5	0.5
144	−0.9	0.9	166	−0.8	0.5
154	−1.0	0.8	183	−0.8	0.5
164	−0.9	0.9	196	−0.9	0.5
169	−0.6	1.1	212	−0.8	0.5
174	−0.9	0.9	226	−0.9	0.5
179	−0.9	0.9	241	−0.6	0.5
184	−0.6	1.1	256	−0.5	0.5
190.5	−0.7	1.0	271	−0.5	0.5
194	−0.7	1.0	286	−0.2	0.5
199	−0.9	0.9	299	−0.7	0.5
204	−1.0	0.8	308	−0.7	0.5
209	−0.8	0.9	316	−0.3	0.5
214	−0.7	1.0	331	−0.4	0.5
232	−0.7	1.0	346	0.0	0.5
240	−0.7	1.0	376	−0.3	0.5
260	−1.5	0.6			

* SST derived after Glemser et al. (2019). ** SSST derived after Kloster et al. (2018).

and low-rectangularity groups seen in glacial sediments by Kloster et al. (2018), but instead they suggest a single morphotype per population that has a mostly moderate rectangularity (around the 0.751 threshold) or is skewed towards high-rectangularity valves as seen in sample BC495.

Like in the Amundsen Sea, we observe unimodal, low-rectangularity trending *F. kerguelensis* populations in Sabrina Coast surface sediments. Means range from 0.731 to 0.743, and medians range from 0.728 to 0.738 and 0.721 to 0.740, which are almost equal and signify normal population. Skew ranges from −1.037 to 1.752, kurtosis ranges from 0.488 to 20.179, and pLR ranges from 0.796 to 0.904. While the mean, median, and mode suggest a normal population, skew and kurtosis suggest that Sabrina Coast sediments are weighted towards low-rectangularity valves (indicated by high pLR) and have outliers.

Kurtosis values differ between *F. kerguelensis* assemblages from the Amundsen Sea and Sabrina Coast. Kurtosis is between −1 and 1 in the Amundsen Sea, suggesting the data are mostly centered around the mean and are close to normal distributions (kurtosis = 0). However, assemblages from the Sabrina Coast display a much higher kurtosis range from 0.488 to 20.179. High kurtosis values indicate the presence of large outliers, in this context suggesting that several *F. kerguelensis* specimens in each Sabrina Coast population may lie far from the mean and have less of a "standard" valve morphology.

These discrepancies in *F. kerguelensis* populations between the sites suggest that the Amundsen Sea and Sabrina Coast have distinctly different *F. kerguelensis* popula-

tions preserved in the surface sediments. If the underlying population dynamics and controls in both geographic regions were the same, it can be reasoned that the populations should be visually and statistically similar, yet they are not. Sabrina Coast *F. kerguelensis* populations contain higher pLR, have wider population distributions and have lower means than do the *F. kerguelensis* populations in the Amundsen Sea. This is another line of questioning that should be interrogated further, although this high pLR distribution off the Sabrina Coast is supported by expected relative abundance of the two morphotypes as modeled by Glemser et al. (2019), who suggested that the biogeographic cline between low and high pLR would be more southerly around the Sabrina Coast than in the Amundsen Sea *F. kerguelensis* and would have proportionally higher pLR. This supports the hypothesis of Glemser et al. (2019) and Kloster et al. (2018) that the border between high and low pLR follows the southern boundary of the Antarctic Circumpolar Current (sbACC; Orsi et al., 1995); the region south of the sbACC is dominated by low pLR, and the region north of the sbACC is dominated by high pLR.

4.3 Regional variability in *F. kerguelensis* populations

There is a clear difference between *F. kerguelensis* in Amundsen Sea vs. Sabrina Coast surface sediments. First, pLR is much lower in the Amundsen Sea than on the Sabrina Coast. In the Amundsen Sea, pLR values are 0.141 (BC495), 0.448 (PC496) and 0.435 (U1532). Off the Sabrina Coast, pLR values range from 0.796 to 0.903 across sites on and off the continental shelf. In situ SST measurements in this area of the Southern Ocean record temperatures between −2 and −1 °C (Bensi et al., 2022; Orsi and Webb, 2022), which is 0.5–1.5 °C colder than in the Amundsen Sea. These cold SSTs should support very low pLR, but *F. kerguelensis* assemblages in the Sabrina Coast surface sediments have high pLR. It is interesting that despite having colder water than the Amundsen Sea, Sabrina Coast assemblages predominantly display low-rectangularity valves when colder waters should display predominantly high-rectangularity valves. While seemingly at odds with the underlying theory that high-rectangularity valves will present themselves in cold waters, it must be noted that the two samples taken from on the Sabrina Coast continental shelf under presumably colder SST, MC45 and MC61, do display lower pLR (0.796 and 0.816), while the continental slope samples, MC01, MC02, MC03 and MC04, display marginally higher pLR (0.877, 0.835, 0.867, 0.904, respectively), with the exception of MC05 (0.809). Despite the fact that Sabrina Coast samples are generally at odds with the Amundsen Sea samples, the Sabrina Coast samples appear to display regional variability that aligns with the idea that higher pLR is found in warmer waters while lower pLR is found at colder waters. Regarding pLR within the Amundsen Sea, samples here also align with the concept of regional variability. The south-

ernmost sample, BC495, displays a pLR of 0.141; PC496 is more northerly and displays a pLR 0.448; and U1532 is northerly still and displays a pLR of 0.435, suggesting that pLR increases moving north presumably as SST warms. Collectively, it appears that *F. kerguelensis* populations display decreasing pLR variability with southerly latitude within regions of the Southern Ocean, but this process is not consistent region to region.

4.4 Drivers of change within *F. kerguelensis*

Here we hypothesize on drivers of change within *F. kerguelensis* that should be tested with further investigation. The observed biogeographic discrepancies may be due to genetic speciation within distinct parts of the Southern Ocean rather than a single, Southern Ocean-wide *F. kerguelensis* species. Postel et al. (2020) identified three genetically distinct strains of *F. kerguelensis* in the Weddell Sea alone. Each of these strains had a latitudinal zonation, i.e., a northern strain and southern strain, as well as an omnipresent strain found throughout the Weddell Sea alongside both groups. The northern strain exhibited the lowest rectangularity, the southern strain exhibited the highest rectangularity, while the omnipresent strain displayed a moderate rectangularity. If the Weddell Sea alone can host three genetically distinct strains of *F. kerguelensis*, then it is reasonable that other parts of the Southern Ocean host their own unique genetic strains. The Sabrina Coast population appears to be most like the omnipresent form identified by Postel et al. (2020) in terms of rectangularity. Consequently, biogeographic differences, as observed in many Southern Ocean diatom groups (Testa et al., 2021), may account for the differences in population rectangularity observed in the Amundsen Sea and Sabrina Coast populations. It is probable that the presentation of two rectangularity morphotypes observed in Kloster et al. (2018) is actually a mixture of the three genetic strains identified by Postel et al. (2020) rather than a single-species population actively changing morphology. It may be possible to differentiate these strains via microscopy and valve rectangularity measurement without having to rely on genetic sequencing techniques.

These genetic differences may be driven by Southern Ocean circulation patterns. The surface waters of the Amundsen Sea Embayment (ASE) lie at the easternmost limb of the clockwise-circulating Ross Sea Gyre (e.g., Assmann et al., 2005; Wåhlin et al., 2012; Gómez-Valdivia et al., 2023) that may have an isolating effect on *F. kerguelensis* populations. It is possible that *F. kerguelensis* in the Amundsen Sea display higher percentages of the "colder water" low-rectangularity specimen because they are restricted to these colder waters circulating within the Ross Sea Gyre. Although a gyre has been documented along the Sabrina Coast (Bindoff et al., 2000), the coastline is much less embayed than ASE, thus *F. kerguelensis* off the Sabrina Coast may not have such oceanographic confinement, likely resulting in less

genetic population isolation. An in-depth study of Sabrina Coast *F. kerguelensis* is required to question why populations would differ from the Amundsen Sea. This hypothesis could be tested through direct sampling of *F. kerguelensis* in the water column in a latitudinal transect from more northerly waters to the Sabrina Coast and comparing population rectangularity to observed SSTs at sampling sites after Glemser et al. (2019). At this time, additional data over a broader geographic scope will allow us to better understand the relationship between *F. kerguelensis* shape, genetic variability and surface water temperature, as well as other oceanographic conditions, in the modern Southern Ocean. Additionally, this work will be improved by comparing *F. kerguelensis* in surface sediment samples to SSTs directly measured at or near the collection site. This will be a valuable test of how *F. kerguelensis* populations in surface sediments compare to those in the water column and how each dataset compares to in situ SST. Given the ubiquitous and dominant occurrence of *F. kerguelensis* in Southern Ocean sediments, a better understanding of the drivers of change within *F. kerguelensis* may allow us to develop regional calibrations between *F. kerguelensis* valve rectangularity and SST that can be used to reconstruct Southern Ocean SSTs over time.

4.5 SST in the Amundsen Sea during the last interglacial period (MIS-5)

Configuration of the WAIS and Southern Ocean conditions during MIS-5 ($\sim$ 130 to 74 ka) have been the subject of debate for many years. Mercer (1978) first suggested that conditions in West Antarctica may have been warm enough to trigger WAIS collapse during MIS-5. Collapse is not a precisely defined term but generally refers to a significant contraction of grounded ice within a short time (Bart and Kratochvil, 2022) that would result in an oceanic connection of the Amundsen, Ross and Weddell seas (Mas e Braga et al., 2021). Before even considering air temperature, such a collapse would likely require a sustained increase in ocean temperature exceeding 2 °C warmer than modern for a period of $\sim$ 1 ka; however, only a 1 °C increase is necessary if sustained over 2 ka, and even less time is needed when air temperature increase is added to the model (Turney et al., 2020; Mas e Braga et al., 2021). Early modeling studies of the MIS-5 Southern Ocean suggested that water temperatures were similar to or only slightly warmer than today (Cline et al., 1984). This early conclusion is supported by a study on marine sediment cores from the Amundsen Sea that found no direct evidence for a WAIS collapse during MIS-5 (Hillenbrand et al., 2002). Furthermore, Southern Ocean SST reconstructions using various methods from different sectors of the Southern Ocean, including the Pacific sector, suggest a slightly warmer MIS-5 with reconstructed SSTs ranging between 0.05–2.5 °C warmer than modern values (Esper and Gersonde, 2014; Chadwick et al., 2020, 2022). In the Atlantic sector, diatom transfer functions reconstructed

maximum MIS-5 SSTs between 0.5 and 2.5 °C warmer than modern (Zielinski et al., 1998; Kunz-Pirrung et al., 2002; Bianchi and Gersonde, 2002). In the Ross Sea, TEX_{86} reconstructed MIS-5e SSTs ~ 2.5 °C warmer than today (Hartman et al., 2021). Although few SST reconstructions exist in the Amundsen Sea, one diatom transfer function reconstruction suggests a warming of only 0.05 °C at core site PS58/271 at 61.24° S, −116.05° E (Esper and Gersonde, 2014; Chadwick et al., 2020, 2022). These studies, although disparate in quantity, suggest that the different SST reconstructions in WAIS drainage areas like the Amundsen Sea and Ross Sea are in agreement that this part of the Southern Ocean was at most ~ 2.5 °C warmer than modern during MIS-5e, the warmest period of MIS-5. Further MIS-5 SST reconstruction efforts will elucidate how warm these bodies were and for how long.

Before we delve into our MIS-5 Amundsen Sea SST reconstruction, it should be noted that downcore temperature reconstruction results should be taken as a cursory investigation of this method and are subject to change upon refinement of this method as a paleotemperature proxy. Although Glemser et al. (2019) notes that *F. kerguelensis* morphotype relative abundance is informative below +3.5 °C, there is not currently a range of error assigned to either the SST or SSST equation. We also switch units from time (ka) to depth below the sea floor (cm b.s.f.), due to a disparity of internal time constraints for this section.

In core PC496, we reconstruct SSTs for MIS-5 between −1.0 to −0.5 °C, which is consistently colder than the modern Amundsen Sea. In core U1533, between the depths 138–256 cm b.s.f. we reconstruct SSTs that are slightly colder than the modern Amundsen Sea range. Below this depth, we derived SSTs that are approximately within the range of the modern Amundsen Sea. U1533 supports the idea that the early part of MIS-5 (MIS-5e) was the warmest part of the interglacial (Bianchi and Gersonde, 2002; Capron et al., 2014; Chadwick et al., 2022). Derived SSTs below 256 cm b.s.f. approach 0 °C and then generally cool moving upwards throughout the stage. Interestingly, we do not reconstruct the warmer MIS-5e trend in the lower depths of PC496, even though the sites are not far from each other (< 150 km). This discrepancy may be caused by several variables, including a larger influence of CDW advected toward the Amundsen Sea margin at the slightly more northerly site U1533 than at site PC496 or a larger influence of cool, glacial meltwater originating from the WAIS margins at the more southerly site PC496. Nonetheless, our results do not indicate that any part of Amundsen Sea MIS-5 was significantly warmer than it is today. Additionally, we do observe SST fluctuations in both cores that may be tied to each of the MIS-5 substages (Shackleton, 1969), although this is speculative at this point with no internal time constraints in the MIS-5 section of either core.

5 Conclusions

In this study, we characterized Amundsen Sea and Sabrina Coast *F. kerguelensis* assemblages in seafloor and downcore sediments using the parameter "rectangularity". We found that surface sediment assemblages in both study locations are different from each other, with Amundsen Sea assemblages displaying moderate- to high-rectangularity valves and Sabrina Coast assemblages predominantly low-rectangularity valves. When we apply equations from Kloster et al. (2018) and Glemser et al. (2019) to derive SSST and SST, respectively, we derive different temperatures. Derived temperatures of the Sabrina Coast are much warmer than those of the Amundsen Sea despite the Sabrina Coast actually being colder than the Amundsen Sea. We hypothesize that this discrepancy reflects distinct dominant genetic strains in the two studied regions that may respond to surface temperature differently. Drivers of population change may also be related to ecological shifts that are not strictly dependent on SST. Our preferred hypothesis is that ocean circulation patterns play the dominant role in maintaining different *F. kerguelensis* genetic populations, which have preferential environmental conditions, such as SST, linked to distinct geographic zones within the Southern Ocean.

We also apply the two equations for deriving SST and SSST across the MIS-5 interval of two Amundsen Sea cores in an investigation into how well this method can be used a temperature proxy. Using these methods, we find that the last interglacial in the Amundsen Sea was colder than or as warm as (but not warmer than) the modern Amundsen Sea. While we have worked to reconstruct such past temperatures in this location using this method, we believe that our understanding of *F. kerguelensis* ecological dynamics is not fully developed. With our new understanding that *F. kerguelensis* populations between different parts of the Southern Ocean are visually and possibly genetically different from each other, it is likely that rectangularity changes do not reflect an "active" response to a changing ocean, rather reflecting a shift in the oceanographic zonation of a specific genetic group that has a preferred environmental regime. It is imperative that intentional steps are taken to further develop our understanding of the drivers of *F. kerguelensis* ecological dynamics and their relationship to SST, as well as other oceanographic conditions, in the Southern Ocean. Developing a better understanding of what drives *F. kerguelensis* population change may allow us to develop regional calibrations so that we can reconstruct the past Southern Ocean as far back as the mid-Pleistocene. Future work should address links between oceanographic and ecologic variables that may govern population change as well as diatom genetic analyses. We contend that rectangularity is a useful and analytically "simple" means of measuring *F. kerguelensis* populations.

References

Assmann, K. M., Hellmer, H. H., and Jacobs, S. S.: Amundsen Sea ice production and transport, J. Geophys. Res.-Ocean., 110, C12013, https://doi.org/10.1029/2004JC002797, 2005.

Bart, P. J. and Kratochvil, M.: A paleo-perspective on West Antarctic Ice Sheet retreat, Sci. Rep., 12, 17693, https://doi.org/10.1038/s41598-022-22450-3, 2022.

Bensi, M., Kovačević, V., Donda, F., O'Brien, P. E., Armbrecht, L., and Armand, L. K.: Water masses distribution offshore the Sabrina Coast (East Antarctica), Earth Syst. Sci. Data, 14, 65–78, https://doi.org/10.5194/essd-14-65-2022, 2022.

Bianchi, C. and Gersonde, R.: The Southern Ocean surface between Marine Isotope Stages 6 and 5d: Shape and timing of climate changes, Palaeogeogr., Palaeoclimatol., 187, 151–177, https://doi.org/10.1016/S0031-0182(02)00516-3, 2002.

Bindoff, N. L., Rosenberg, M. A., and Warner, M. J.: On the circulation and water masses over the Antarctic continental slope and rise between 80 and 150° E, Deep-Sea Res. Pt. II, 47, 2299–2326, https://doi.org/10.1016/S0967-0645(00)00038-2, 2000.

Capron, E., Govin, A., Stone, E. J., Masson-Delmotte, V., Mulitza, S., Otto-Bliesner, B., Rasmussen, T. L., Sime, L. C., Waelbroeck, C., and Wolff, E. W.: Temporal and spatial structure of multi-millennial temperature changes at high latitudes during the Last Interglacial, Quaternary Sci. Rev., 103, 116–133, https://doi.org/10.1016/j.quascirev.2014.08.018, 2014.

Chadwick, M., Allen, C. S., Sime, L. C., and Hillenbrand, C. D.: Analysing the timing of peak warming and minimum winter sea-ice extent in the Southern Ocean during MIS 5e, Quaternary Sci. Rev., 229, 106134, https://doi.org/10.1016/j.quascirev.2019.106134, 2020.

Chadwick, M., Allen, C. S., Sime, L. C., Crosta, X., and Hillenbrand, C.: How does the Southern Ocean palaeoenvironment during Marine Isotope Stage 5e compare to the modern?, Mar. Micropaleontol., 170, 102066, https://doi.org/10.1016/j.marmicro.2021.102066, 2022.

Cline, R. M. L., Ruddiman, W. F., Hays, J. D., Prell, W. L., Moore, T. C., Kipp, N. G., Molfino, B. E., Denton, G. H., and Hughes, T. J.: The Last Interglacial Ocean, Quaternary Res., 21, 123–224, https://doi.org/10.1016/0033-5894(84)90098-X, 1984.

Cortese, G. and Gersonde, R.: Morphometric variability in the diatom Fragilariopsis kerguelensis: Implications for Southern Ocean paleoceanography, Earth Planet Sc. Let., 257, 526–544, https://doi.org/10.1016/j.epsl.2007.03.021, 2007.

Cortese, G. and Gersonde, R.: Plio/Pleistocene changes in the main biogenic silica carrier in the Southern Ocean, Atlantic Sector, Mar. Geol., 252, 100–110, https://doi.org/10.1016/j.margeo.2008.03.015, 2008.

Cortese, G., Gersonde, R., Maschner, K., and Medley, P.: Glacial-interglacial size variability in the diatom *Fragilariopsis kerguelensis*: Possible iron/dust controls?: DIATOM SIZE VARIABILITY, Paleoceanography, 27, PA1208, https://doi.org/10.1029/2011PA002187, 2012.

Crosta, X.: Holocene size variations in two diatom species off East Antarctica: Productivity vs environ-

mental conditions, Deep-Sea Res. Pt. I, 56, 1983–1993, https://doi.org/10.1016/j.dsr.2009.06.009, 2009.

de Bar, M. W., Weiss, G., Yildiz, C., Rampen, S. W., Lattaud, J., Bale, N. J., Mienis, F., Brummer, G. J. A., Schulz, H., Rush, D., Kim, J. H., Donner, B., Knies, J., Luckge, A., Stuut, J. B. W., Damste, J. S. S., and Schouten, S.: Global temperature calibration of the Long chain Diol Index in marine surface sediments, Org. Geochem., 142, 103983, https://doi.org/10.1016/j.orggeochem.2020.103983, 2020.

DeConto, R. M. and Pollard, D.: Contribution of Antarctica to past and future sea-level rise, Nature, 531, 591–597, https://doi.org/10.1038/nature17145, 2016.

Droop, S.: A morphometric and geographical analysis of two races of *Diploneis smithii*/*D. fusca* (Bacillariophyceae) in Britain, edited by: Marino, D. and Montresor, M., 347–369, 1995.

Enderlein, P. and Larter, R. D.: Cruise Report JR 179, RRS James Clark Ross, February to April 2008, https://www.bodc.ac.uk/resources/inventories/cruise_inventory/report/8277/ (last access: 1 June 2024), 2008.

Esper, O. and Gersonde, R.: Quaternary surface water temperatrue estimations: New diatom transfer functions for the Southern Ocean, Palaeogeogr., Palaeoclimatol., 414, 1–19, https://doi.org/10.1016/j.palaeo.2014.08.008, 2014.

Fietz, S., Ho, S. L., Huguet, C., Rosell-Melé, A., and Martínez-García, A.: Appraising GDGT-based seawater temperature indices in the Southern Ocean, Org. Geochem., 102, 93–105, https://doi.org/10.1016/j.orggeochem.2016.10.003, 2016.

Glemser, B., Kloster, M., Esper, O., Eggers, S. L., Kauer, G., and Beszteri, B.: Biogeographic differentiation between two morphotypes of the Southern Ocean diatom Fragilariopsis kerguelensis, Polar Biol., 42, 1369–1376, https://doi.org/10.1007/s00300-019-02525-0, 2019.

Gohl, K., Wellner, J. S., Klaus, A., Bauersachs, T., Bohaty, S. M., Courtillat, M., Cowan, E. A., De Lira Mota, M. A., Esteves, M. S. R,. Fegyveresi, J. M, Frederichs, T., Gao, L., Halberstadt, A. R., Hillenbrand, C.-D., Horikawa, K., Iwai, M., Kim, J. H., King, T. M., Klages, J. P., Passchier, S., Penkrot, M. L., Prebble, J. G., Rahaman, W., Reinardy, B. T. I., Renaudie, J., Robinson, D. E., Scherer, R. P., Siddoway, C. S., Wu, L., and Yamane, M.: Expedition 379 summary, Proc. IODP, v. 379, p. 21, 2021.

Gómez-Valdivia, F., Holland, P., Siahaan, A., Dutrieux, P., and Young, E.: Projected West Antarctic Ocean Warming Caused by an Expansion of Ross Gyre, Geophys. Res. Lett., 50, e2023GL102978, https://doi.org/10.1029/2023GL102978, 2023.

Hartman, J. D., Sangiorgi, F., Barcena, M. A., Tateo, F., Giglio, F., Albertazzi, S., Trincardi, F., Bijl, P. K., Langone, L., and Asioli, A.: Sea-ice, primary productivity and ocean temperatures at the Antarctic marginal zone during late Pleistocene, Quaternary Sci. Rev., 266, 107069, https://doi.org/10.1016/j.quascirev.2021.107069, 2021.

Hillenbrand, C.-D., Smith, J. A., Hodell, D. A., Greaves, M., Poole, C. R., Kender, S., Williams, M., Andersen, T. J., Jernas, P. E., Elderfield, H., Klages, J. P., Roberts, S. J., Gohl, K., Larter, R. D., and Kuhn, G.: West Antarctic Ice Sheet retreat driven by Holocene warm water incursions, Nature, 547, 43–48, https://doi.org/10.1038/nature22995, 2017.

Hillenbrand, C.-D., Fütterer, D., Grobe, H., and Frederichs, T.: No evidence for a Pleistocene collapse of the West Antarctic Ice Sheet from continental margin sediments recovered in the Amundsen Sea, Geo-Mar. Lett., 22, 51–59, https://doi.org/10.1007/s00367-002-0097-7, 2002.

Ho, S. L., Mollenhauer, G., Fietz, S., Martinez-Garcia, A., Lamy, F., Rueda, G., Schipper, K., Mehuest, M., Rosell-Mele, A., Stein, R., and Tiedemann, R.: Appraisal of TEX_{86} and TEX_{86}^{L} thermometries in subpolar and polar regions, Geochim. Cosmochim. Ac., 131, 213–226, https://doi.org/10.1016/j.gca.2014.01.001, 2014.

Holland, D. M., Nicholls, K. W., and Basinski, A.: The Southern Ocean and its interaction with the Antarctic Ice Sheet, Science, 367, 1326–1330, https://doi.org/10.1126/science.aaz5491, 2020.

Hopkins, B., Xuan, C., Hillenbrand, C.-D., Van Peer, T. E., Jin, Y., Frederichs, T., Gao, L., and Bohaty, S. M.: Evaluation of geomagnetic relative palaeointensity as a chronostratigraphic tool in the Southern Ocean: Refined Plio-/Pleistocene chronology of IODP Site U1533 (Amundsen Sea, West Antarctica), Quaternary Sci. Rev., 325, 108460, https://doi.org/10.1016/j.quascirev.2023.108460, 2024.

Horrocks, J.: The formation and late Quaternary palaeoenviornmental history of sediment mounds in the Amundsen Sea, West Antarctica, Thesis, Durham University, http://etheses.dur.ac.uk/12659/ (last access: 27 June 2024), 2018.

Inglis, G. N. and Tierney, J. E.: The TEX86 Paleotemperature Proxy, Cambridge University Press, https://doi.org/10.1017/9781108846998, 2020.

Kim, J.-H., Crosta, X., Michel, E., Schouten, S., Duprat, J., and Sinninghe Damsté, J. S.: Impact of lateral transport on organic proxies in the Southern Ocean, Quaternary Res., 71, 246–250, https://doi.org/10.1016/j.yqres.2008.10.005, 2009.

Kloster, M., Kauer, G., and Beszteri, B.: SHERPA: an image segmentation and outline feature extraction tool for diatoms and other objects, BMC Bioinformatics, 15, p. 218, https://doi.org/10.1186/1471-2105-15-218, 2014.

Kloster, M., Esper, O., Kauer, G., and Beszteri, B.: Large-Scale Permanent Slide Imaging and Image Analysis for Diatom Morphometrics, Appl. Sci., 7, p. 330, https://doi.org/10.3390/app7040330, 2017.

Kloster, M., Kauer, G., Esper, O., Fuchs, N., and Beszteri, B.: Morphometry of the diatom Fragilariopsis kerguelensis from Southern Ocean sediment: High-throughput measurements show second morphotype occurring during glacials, Mar. Micropaleontol., 143, 70–79, https://doi.org/10.1016/j.marmicro.2018.07.002, 2018.

Kunz-Pirrung, M., Gersonde, R., and Hodell, D. A.: Mid-Brunhes century-scale diatom sea surface temperature and sea ice records from the Atlantic sector of the Southern Ocean (ODP Leg 177, sites 1093, 1094 and core PS2089-2), Palaeogeogr., Palaeoclimatol., 182, 305–328, https://doi.org/10.1016/S0031-0182(01)00501-6, 2002.

Lisiecki, L. E. and Raymo, M. E.: A Pliocene-Pleistocene stack of 57 globally distributed benthic $\delta^{18}O$ records, PLIOCENE-PLEISTOCENE BENTHIC STACK, Paleoceanography, 20, PA1003, https://doi.org/10.1029/2004PA001071, 2005.

Locarnini, R. A., Mishonov, A. V., Antonov, J. I., Boyer, T. P., Garcia, H. E., Baranova, O. K., Zweng, M. M., and Johnson, D. R.: World Ocean Atlas 2009, Vol. 1, Temperature, edited by: O. C. L. National Oceanographic Data Center (U.S.) & N. E. S. United States Data, and Information Service, https://doi.org/10.7289/V55X26VD, 2009.

Locarnini, R. A., Mishonov, A. V., Antonov, J. I., Boyer, T. P., Garcia, H. E., Baranova, O. K., Zweng, M. M., Paver, C. R., Reagan, J. R., Johnson, D. R., Hamilton, M., and Seidov, D.: World Ocean Atlas 2013, Volume 1, Temperature, O. C. L. National Oceanographic Data Center (U.S.) and N. E. S. United States Data, and Information Service, https://doi.org/10.7289/V55X26VD, 2013.

Martinson, D. G., Stammerjohn, S. E., Iannuzzi, R. A., Smith, R. C., and Vernet, M.: Western Antarctic Peninsula physical oceanography and spatio–temporal variability, Deep-Sea Res. Pt. II, 55, 1964–1987, https://doi.org/10.1016/j.dsr2.2008.04.038, 2008.

Mas e Braga, M., Bernales, J., Prange, M., Stroeven, A. P., and Rogozhina, I.: Sensitivity of the Antarctic ice sheets to the warming of marine isotope substage 11c, The Cryosphere, 15, 459–478, https://doi.org/10.5194/tc-15-459-2021, 2021.

Matsuoka, K., Skoglund, A., Roth, G., de Pomereu, J., Griffiths, H., Headland, R., Herried, B., Katsumata, K., Le Brocq, A., Licht, K., Morgan, F., Neff, P. D., Ritz, C., Scheinert, M., Tamura, R., Ven de Putte, A., van den Broeke, M., von Deschwanden, A., Deschamps-Berger, C., Van Liefferinge, B., Tronstad, S., and Melvaer, Y.: Quantarctica, an integrated mapping environment for Antarctica, the Southern Ocean, and sub-Antarctic islands, Environ. Model. Softw., 140, 105015, https://doi.org/10.1016/j.envsoft.2021.105015, 2021.

Mercer, J.: West Antarctic ice sheet and CO_2 greenhouse effect: a threat of disaster, Nature, 271, 321–325, https://doi.org/10.1038/271321a0, 1978.

Mollenhauer, G., Basse, A., Kim, J.-H., Sinninghe Damsté, J. S., and Fischer, G.: A four-year record of $U_{37}^{K'}$ – and TEX_{86}-derived sea surface temperature estimates from sinking particles in the filamentous upwelling region off Cape Blanc, Mauritania, Deep-Sea Res. Pt. I, 97, 67–79, https://doi.org/10.1016/j.dsr.2014.11.015, 2015.

Morlighem, M., Rignot, E., Binder, T., et al.: Deep glacial troughs and stabilizing ridges unveiled beneath the margins of the Antarctic ice sheet, Nat. Geosci., 13, 132–137, https://doi.org/10.1038/s41561-019-0510-8, 2020.

Orsi, A. H. and Webb, C. J.: Impact of Sea Ice Production off Sabrina Coast, East Antarctica, Geophys. Res. Lett., 49, e2021GL095613, https://doi.org/10.1029/2021GL095613, 2022.

Orsi, A., Whitworth III, T., and Nowlin Jr., W.: On the meridional extent and fronts of the Antarctic Circumpolar Current, Deep-Sea Res. Pt. I, 42, 641–673, https://doi.org/10.1016/0967-0637(95)00021-W, 1995.

Patterson, M. O., Levy, R. H., Kulhanek, D. K., van de Flierdt, T., Horgan, H., Dunbar, G. B., Naish, T. R., Ash, J., Pyne, A., Mandeno, D., Winberry, P., Harwood, D. M., Florindo, F., Jimenez-Espejo, F. J., Läufer, A., Yoo, K.-C., Seki, O., Stocchi, P., Klages, J. P., Lee, J. I., Colleoni, F., Suganuma, Y., Gasson, E., Ohneiser, C., Flores, J.-A., Try, D., Kirkman, R., Koch, D., and the SWAIS 2C Science Team: Sensitivity of the West Antarctic Ice Sheet to +2 °C (SWAIS 2C), Sci. Dril., 30, 101–112, https://doi.org/10.5194/sd-30-101-2022, 2022.

Postel, U., Glemser, B., Salazar Aleksayeva, K., Lena Eggers, S., Groth, M., Glockner, G., Uwe, J., Mock, T., Klemm, K., Valentin, K., and Besteri, B.: Adaptive divergence across Southern Ocean gradients in the pelagic diatom *Fragilariopsis kerguelensis*, Mol. Ecol., 29, 4913–4924, https://doi.org/10.1111/mec.15554, 2020.

Ruggiero, J.: Population morphometrics of the Southern Ocean diatom Fragilariopsis kerguelensis related to Sea Surface Temperature, U.S. Antarctic Program (USAP) Data Center [data set], https://doi.org/10.15784/601804, 2024.

Seroussi, H., Nakayama, Y., Larour, E., Menemenlis, D., Morlighem, M., Rignot, E., and Khazendar, A.: Continued retreat of Thwaites Glacier, West Antarctica, controlled by bed topography and ocean circulation, ICE-OCEAN MODELING OF THWAITES GLACIER, Geophys. Res. Lett., 44, 6191–6199, https://doi.org/10.1002/2017GL072910, 2017.

Shackleton, N. J.: The last interglacial in the marine and terrestrial records, Proc. Roy. Soc. Lond. Ser. B, 174, 135–154, https://doi.org/10.1098/rspb.1969.0085, 1969.

Shukla, S. K. and Crosta, X.: *Fragilariopsis kerguelensis* size variability from the Indian subtropical Southern Ocean over the last 42 000 years, Ant. Sci., 29, 139–146, https://doi.org/10.1017/S095410201600050X, 2017.

Shukla, S. K., Crosta, X., Cortese, G., and Nayak, G. N.: Climate mediated size variability of diatom Fragilariopsis kerguelensis in the Southern Ocean, Quaternary Sci. Rev., 69, 49–58, https://doi.org/10.1016/j.quascirev.2013.03.005, 2013.

Testa, G., Piñones, A., and Castro, L. R.: Physical and Biogeochemical Regionalization of the Southern Ocean and the CCAMLR Zone 48.1, Front. Mar. Sci., 8, 592378, https://doi.org/10.3389/fmars.2021.592378, 2021.

Turney, C. S. M., Fogwill, C. J., Golledge, N., R., McKay, N. P., van Sebille, E., Jones, R. T., Etheridge, D., Rubino, M., Thornton, D. P., Davies, S. M., Bronk Ramsey, C., Thomas, Z. A., Bird, M. I., Munksgaard, N. C., Kohno, M., Woodward, J., Winter, K., Weyrich, L. S., Rootes, C. M., and Millman, H.: Early Last Interglacial ocean warming drove substantial ice mass loss from Antarctica, P. Natl. Acad. Sci. USA, 117, 3996–4006, https://doi.org/10.1073/pnas.1902469117, 2020.

Uenzelmann-Neben, G. and Gohl, K.: Amundsen Sea sediment drifts: Archives of modifications in oceanographic and climatic conditions, Mar. Geol., 299–302, 51–62, https://doi.org/10.1016/j.margeo.2011.12.007, 2012.

Wåhlin, A. K., Muench, R. D., Arneborg, L., Björk, G., Ha, H. K., Lee, S. H., and Alsén, H.: Some Implications of Ekman Layer Dynamics for Cross-Shelf Exchange in the Amundsen Sea, J. Phys. Oceanogr., 42, 1461–1474, https://doi.org/10.1175/JPO-D-11-041.1, 2012.

Warnock, J. P. and Scherer, R. P.: A revised method for determining the absolute abundance of diatoms, J. Paleolim., 53, 157–163, https://doi.org/10.1007/s10933-014-9808-0, 2015.

Zielinski, U., Gersonde, R., Sieger, R., and Fütterer, D.: Quaternary surface water temperature estimations, Calibration of a diatom transfer function for the Southern Ocean, Paleoceanography, 13, 365–383, https://doi.org/10.1029/98PA01320, 1998.